

A New Polarized Image Fusion Algorithm Based on Two-scale Guided Filtering

Fei Xie and Jiajia Chen*

Nanjing University of Aeronautics and Astronautics, Nanjing, China

*Corresponding author email: jiajia_chen@nuaa.edu.cn

Abstract—This paper proposes a new fusion algorithm based on two-scale guided filtering for polarized images. After generating the detail and base layers from source image, we construct the saliency map. It provides good characterization of the saliency level information, which is beneficial to the fusion. Subsequently, two different scales of guided filtering are performed on the weight map which is derived from the saliency map. Finally, weighted fusion method is used with the filtered weight map to fuse the detail layer and the base layer. In the proposed algorithm, we improve the saliency map by combining second-order and first-order difference edge detection operations. The weight maps constructed with the improved saliency map can fulfill the requirements of the new weighted fusion method. Compared with the original method, all of the benchmarks on testing images have been significantly improved during objective evaluation. Subjectively, it is also shown that the details of the improved saliency map have become obviously sharper.

Keywords—*image fusion, guided filtering, saliency map, Laplacian operator*

I. INTRODUCTION

Polarization imaging technique can provide more information about the roughness, texture and material of the object surface than traditional optical imaging. Therefore, it has been widely used in military reconnaissance [1], remote sensing detection, medical treatment [2] and astronomical observations. The traditional polarization image analysis mainly interprets information by calculating the Stokes images. However, analyzing individual Stokes image is easy to lose details and could not fully reflect the target polarization information [3]. With the information redundancy and complementarity between polarized images, researchers have proposed a number of polarization information analysis methods based on image fusion technique in the recent years. The objective is to fuse together information that is different and complementary [4].

Li [5] developed a new algorithm for polarization image fusion based on bidimensional empirical mode decomposition (BEMD) and adaptive the pulse-coupled neural network (PCNN). This fusion algorithm combines the advantages of both the multi-resolution and multi-scale characteristic of BEMD transform, as well as the pulse synchronization excitation of PCNN. It successfully solves the problems in traditional polarization image fusion, such as poor visual effect and insufficient detail information. Another group of image fusion methods is based on multi-scale transformation, which apply different fusion strategies to the frequency coefficients of

different scales. The representative algorithms in this group include curvelet transform (CVT) [6], dual-tree complex wavelet transform (DTCWT) [7], and non-subsampled shearlet transform (NSST) [8]. This can achieve more detailed fusion, and therefore has been widely used. However, due to imperfect fusion rules, it is impossible to transfer all the desired information to the fusion image. In addition, these methods may produce brightness and color distortions because spatial consistency is not well considered.

To make full use of spatial context, optimization-based image fusion approaches, e.g., generalized random walks [9], and Markov random fields [10], have been proposed. However, optimization-based methods have a common limitation, i.e., inefficiency, since they require multiple iterations to find the global optimal solution. Moreover, another drawback is that global optimization-based methods may over-smooth the resulting weights, which is not good for fusion. Subsequently, a novel image fusion approach has been proposed in [11] based on random walks fusion framework developed in [10]. Although the complexity of this method is reduced, the ability to retain details in smooth areas is weak. In order to improve efficiency and special consistency, the authors of [12] proposed a new image fusion method with guided filtering. A simple average filter is used to quickly decompose the image into two scales. Although the method of decomposition is simplified, excessive smoothing causes the loss of detailed image information. In addition, a novel weight construction method [12] is proposed to combine pixel saliency and spatial context for image fusion. Instead of using optimization-based methods, guided filtering [13] is adopted as a local filtering method for image fusion. Laplacian operator is used to detect edge information in constructing pixel saliency. However, the edge direction estimation, edge continuity and noise robustness of this algorithm are relatively weak.

In order to address the above challenges, we propose a new fusion algorithm. When constructing the saliency map, we combine Sobel edge detection and Laplacian sharpening. Sobel algorithm is insensitive to noise and provides accurate edge directions, while Laplacian filter has high accuracy in edge positioning. In our algorithm, the polarized images with four angles are used as the source images, which are firstly decomposed into base layer and detail layer. Secondly, the saliency map is improved to construct weight map. At last, guided filtering with the modified parameters is used as local filtering for image fusion. Experimental results show that the proposed method can provide better fusion quality than guided filtering-based fusion (GFF) [12].

The following paper is organized as follows. In Section II, the review about guided filtering is presented. In Section III, the proposed algorithm is introduced with details. In Section IV, the proposed method is compared with GFF and the results of both fusion quality and processing time are presented. Conclusion is presented in Section V.

II. GUIDED FILTERING

In theory, the guided filter assumes that the filtering output O is a linear transformation of the guidance image I , as shown in (1), in a local window W_k centered at pixel k ,

$$O_i = a_k I_i + b_k, \quad \forall i \in W_k \quad (1)$$

where W_k is a square window with size of $(2r+1) \times (2r+1)$.

The linear coefficients a_k and b_k are constant in W_k , which can be estimated by minimizing the squared difference between O and the input image P , as:

$$E(a_k, b_k) = \sum_{i \in W_k} ((a_k I_i + b_k - P_i)^2 + \varepsilon a_k^2) \quad (2)$$

where ε is a regularization parameter given by the user. The coefficients a_k and b_k can be directly solved by linear regression as follows:

$$a_k = \frac{\frac{1}{|W|} \sum_{i \in W_k} I_i P_i - \mu_k \bar{P}}{\delta_k + \varepsilon} \quad (3)$$

$$b_k = \bar{P}_k - a_k \mu_k \quad (4)$$

where μ_k and δ_k are the mean and variance of I in W_k respectively, $|W|$ is the number of pixels in W_k , and \bar{P}_k is the mean of P in W_k . Next, the output image can be calculated by computing the average of a_k and b_k , as follows:

$$O_i = \bar{a}_i I_i + \bar{b}_i \quad (5)$$

$$\bar{a}_i = \frac{1}{|W|} \sum_{k \in W_i} a_k; \quad \bar{b}_i = \frac{1}{|W|} \sum_{k \in W_i} b_k \quad (6)$$

In this paper, $G_{r,\varepsilon}(P,I)$ is used as the function to represent the guided filtering operation. r and ε are the parameters which decide the filter size and blur degree of the guided filter.

The edge-preserving characteristic of guided filter can be intuitively interpreted as follows. When the guided filter is used as an edge-preservation filter, the input image P can be used as the guidance image I , that is, $I=P$. According to (1), (3) and (4), it can be seen that in the flat area, local variance δ_k is very small which means that the pixels in guidance image I remains almost unchanged in W_k . Therefore, a_k becomes close to 0 and the filtering output O equals to \bar{P}_k , i.e., the average of the adjacent input pixels. In contrast, if the local variance is very large which means that the pixels are in an edge area, a_k becomes much greater than zero. As demonstrated in [13], $\nabla O \approx \bar{a} \nabla I$ becomes valid, which means that only the weights in one side of the edge will be averaged. In this way, the edges in I can be preserved in the output O after the filtering.

III. THE PROPOSED METHOD

Due to the edge-preserving properties of guided filtering, we choose guided filtering to perform decomposition and weight map construction to generate the fused base layer and detail layer. Fig. 1 summarizes the main processes of the proposed method. Firstly, we perform self-guided filtering on the source images to get the two-scale representations. Next, we combine the Sobel operation and the Laplacian operation to

improve the saliency map construction. Subsequently, the weight map determined by improved saliency map is used as the input of guided filtering to construct the new weight map. The last but not the least, the base and detail layers are fused by using a guided filtering based method. It uses weighted average to achieve two-scale reconstruction.

A. Two-Scale Image Decomposition

As shown in Fig. 1 A, each source image is decomposed into two scales by guided filter. The base layer can be derived from:

$$B_i = G_{r,\varepsilon_i}(I_i, I_i) \quad (7)$$

$G_{r,\varepsilon_i}(I_i, I_i)$ represents that guided filtering is performed on I_i with I_i also serving as the guidance image, where B_i is the base layer image, I_i is the source image, $i \in \{0^\circ, 45^\circ, 90^\circ, 135^\circ\}$. r and ε_i are the parameters used in guided filtering, and we set $r = 15$, $\varepsilon_i = \sigma_i$, where σ_i is the standard deviation of I_i . Parameter r controls the size of the local window, and the larger window size makes the filtered image to be smoother. However, excessively smoothed basic layer cannot represent the basic information well. On the other hand, when r is too small, it cannot filter out details effectively. According to Cao et al. [14] and our experiments, we set $r = 15$. As proposed in [15], ε_i is selected to be σ_i as the regularization parameter of self-guided filtering. This not only generates a smooth image, but also has better edge-preserving characteristics and spatial consistency than average filter used in GFF. Therefore, the detail layer image D_i can be obtained by subtracting the base layer from the source image, as

$$D_i = I_i - B_i \quad (8)$$

B. Improved Saliency Map Construction

As shown in Fig. 1 B, the saliency map is constructed as follows. Firstly, we use Laplacian filter to highlight details in source images.

$$H_i = I_i * L' \quad (9)$$

where L' is a 3×3 modified Laplacian filter, H_i is derived by the convolution of L' and the source image. As shown in (10), L is the Laplacian filter used in GFF. L' as shown in (11) is used as the Laplacian filter in this paper. Unlike L , which only performs along horizontal and vertical directions, L' also includes 45° and -45° directions. Hence, compared with L , L' has better effect on edge detection [16].

$$L = \begin{bmatrix} 0 & 1 & 0 \\ 1 & -4 & 1 \\ 0 & 1 & 0 \end{bmatrix} \quad (10)$$

$$L' = \begin{bmatrix} 1 & 1 & 1 \\ 1 & -8 & 1 \\ 1 & 1 & 1 \end{bmatrix} \quad (11)$$

Secondly, the sharpened image E_i is obtained by adding the absolute value of H_i to I_i , as

$$E_i = |H_i| + I_i \quad (12)$$

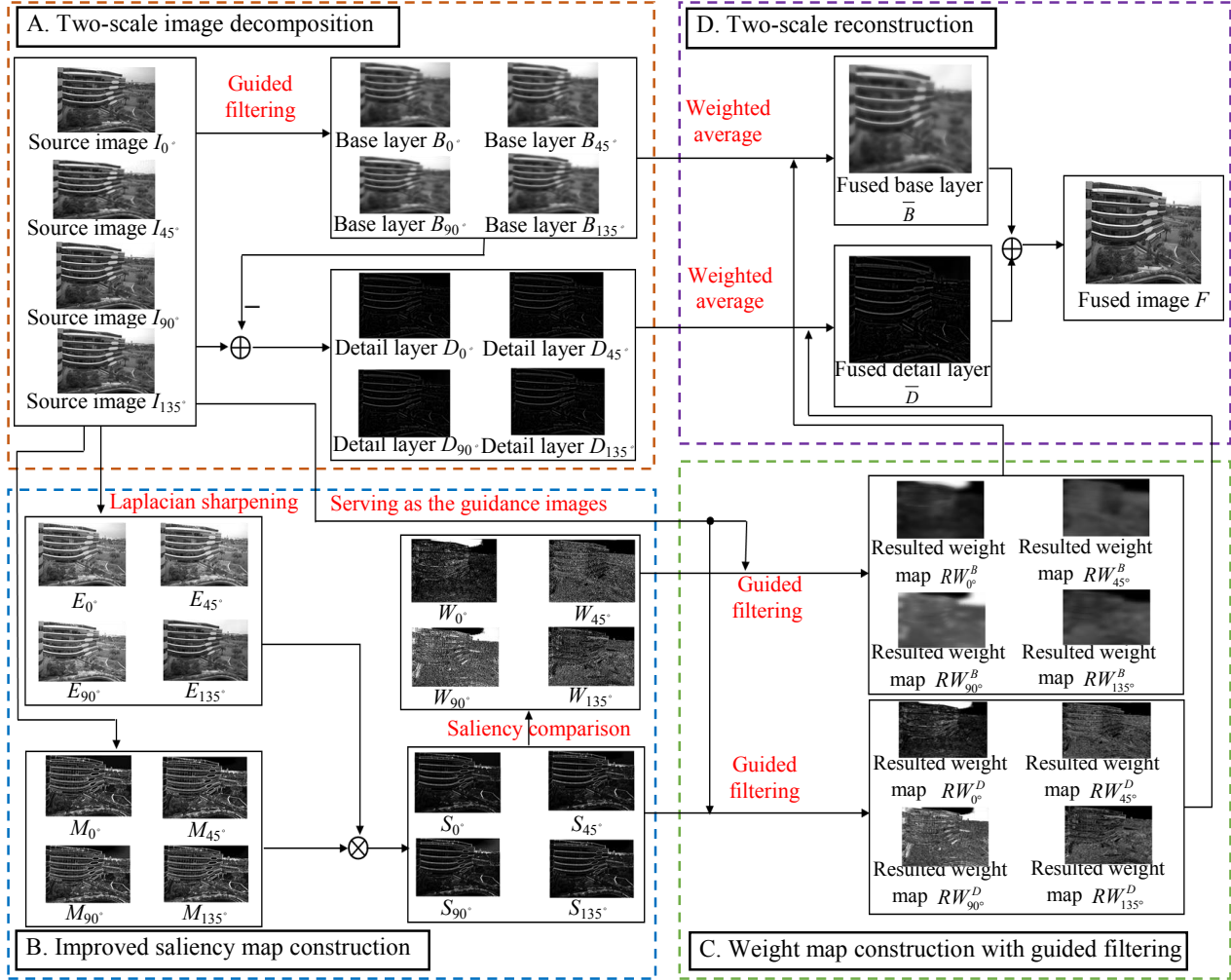


Fig.1 The flowchart of the proposed method

Thirdly, Sobel filter [17] is applied to each source image. It can be achieved as follows:

$$S_h = \begin{bmatrix} -1 & 0 & 1 \\ -2 & 0 & 2 \\ -1 & 0 & 1 \end{bmatrix}, \quad S_v = \begin{bmatrix} -1 & -2 & -1 \\ 0 & 0 & 0 \\ 1 & 2 & 1 \end{bmatrix}$$

$$F_{h,i}(x, y) = \sum_{m=1}^3 \sum_{n=1}^3 I_i(x+m-2, y+n-2) \times S_h(m, n) \quad (13)$$

$$F_{v,i}(x, y) = \sum_{m=1}^3 \sum_{n=1}^3 I_i(x+m-2, y+n-2) \times S_v(m, n)$$

$$F_i(x, y) = |F_{h,i}(x, y)| + |F_{v,i}(x, y)|$$

where h represents horizontal direction and v represents vertical direction. S_h and S_v are Sobel mask for x and y components. (x, y) represents the pixel position in image. $F_{h,i}$ is derived by the convolution of I_i and S_h . $F_{v,i}$ is similarly derived. F_i is calculated by adding the absolute values of $F_{h,i}$ and $F_{v,i}$.

Fourthly, as shown in equation (14), F_i is smoothed by the average filter. The size of average mask A provided by the average filter is conventionally set to 5×5 .

$$M_i = F_i * A \quad (14)$$

Fifthly, as shown in (15), the saliency map S_i is derived by multiplying the smoothed result M_i and the sharpened image E_i . In this case, the smoothed Sobel filtered image can be regarded as a masked image.

$$S_i = M_i \times E_i \quad (15)$$

Finally, the saliency maps are compared to determine the weight maps as

$$W_i^k = \begin{cases} 1 & \text{if } S_i^k = \max(S_{0^\circ}^k, S_{45^\circ}^k, S_{90^\circ}^k, S_{135^\circ}^k) \\ 0 & \text{otherwise} \end{cases} \quad (16)$$

where S_i^k is the saliency value of the pixel k in the saliency map S_i .

C. Weight Map Construction with Guided Filtering

However, as shown in Fig.1 B, weight maps obtained above are usually noisy and not aligned with object boundaries, which may produce artifacts to the fused image. Using spatial consistency is an effective way to solve this problem. Due to the edge-preserving of the guided filtering, those pixels with similar color or brightness tend to have similar weights if we use guided filtering. This is exactly the principle of spatial consistency.

Hence, as shown in Fig. 1 C, guided image filtering is performed on each weight map W_i with the source image I_i serving as the guidance image, as follows:

$$RW_i^B = G_{r_1, \varepsilon_1}(W_i, I_i) \quad (17)$$

$$RW_i^D = G_{r_2, \varepsilon_2}(W_i, I_i) \quad (18)$$

where $r_1, \varepsilon_1, r_2, \varepsilon_2$ are the parameters of guided filter, RW_i^B and RW_i^D are the resulted weight maps of the base and detail layers. Finally, the values of 4 weight maps are normalized.

Furthermore, as shown in Fig.1 A, the base layers look spatially smooth and the detail layers look spatially sharp. Therefore, a large filter size and a large blur degree are preferred for fusing the base layers, while a small filter size and a small blur degree are preferred for fusing the detail layers. Otherwise, artificial edges may be produced. In order to select the size and blur degree of the filter, in this paper, we refine the value range and conduct experiments separately. When $r_1 = 40$, $\varepsilon_1 = 0.3$, $r_2 = 6$, $\varepsilon_2 = 10^{-6}$, the algorithm produces better effect.

D. Two-scale Image Reconstruction

As shown in Fig. 1 D, two-scale image reconstruction consists of the following two steps. Firstly, the base and detail layers of different source images are fused together by weighted averaging, as follows:

$$\bar{B} = \sum_{i=1}^N W_i^B B_i \tag{19}$$

$$\bar{D} = \sum_{i=1}^N W_i^D D_i \tag{20}$$

Secondly, the fused image F is obtained by adding the fused base layer \bar{B} with the fused detail layer \bar{D} .

$$F = \bar{B} + \bar{D} \tag{21}$$

IV. EXPERIMENTAL RESULTS AND DISCUSSION

In this section, the proposed method is compared with GFF [12]. Firstly, various benchmarks are used to objectively evaluate these two methods. Next, subjective evaluation is performed on the saliency map. At last, the processing time of these two methods is evaluated.

A. Objective Evaluation Using Benchmarks

In this session, four images are used to compare the fused image quality of the proposed method with GFF. For these testing, four fusion quality metrics, i.e., information theory based metric (Q_{MI} [18]), structure based metrics (Q_Y [19] and Q_C [20]) and feature based metrics (Q_P [21]) are adopted.

TABLE I. BENCHMARKS OF FOUR ALGORITHMS

Image	Bench mark	GFF [12]	Proposed
	Q_{MI}	0.9308	0.9546
	Q_Y	0.5112	0.5168
	Q_C	0.2255	0.2839
	Q_P	0.7780	0.8498
	Q_{MI}	0.8420	0.8708
	Q_Y	0.4619	0.4851
	Q_C	0.7889	0.8804
	Q_P	0.6623	0.7396
	Q_{MI}	0.7893	0.7970
	Q_Y	0.4885	0.4958
	Q_C	0.7442	0.7446
	Q_P	0.7647	0.7967
	Q_{MI}	0.8562	0.9177
	Q_Y	0.5303	0.5403
	Q_C	0.7186	0.8010
	Q_P	0.8440	0.8783

Table I shows the comparisons of benchmarks between the proposed method and GFF. From Table I, we can conclude that the proposed method performs better in all benchmarks. Q_{MI} defines a measure to objectively evaluate pixel-level fusion performance by evaluating the amount of the original information transferred from the different source images to the fused image. GFF has a lower Q_{MI} score than the proposed method, because the average filter is used in GFF to decompose the image into the base layer and the detail layer. However, it causes blurring and loss of image information such as contrast, background edges and details. Structure based metrics Q_C and Q_Y estimate how well the important information in the source images is preserved in the fused image. When constructing weight maps in our method, the guided filtering with modified parameters is used to generate the resulted weight maps, so that the proposed method can better preserve the complementary information of source images without producing artifacts and distortions. Feature based metric Q_P measures the image characteristics through phase consistency and its corresponding moment. The main moments with consistent phases contain angle and edge information. The construction of saliency maps in this paper can be regarded as a combination of Laplacian filter and Sobel filter. Strong edges and the reduction of visible noise are the key characteristics of masking Laplacian filtered images with a smoothed gradient image. Hence, the proposed method produces better results. To further compare the quality of fused images by GFF and the proposed method, subjective evaluation is done in the next session.

B. Subjective Evaluation on the Saliency Map

The main difference between GFF and the proposed method is constructing saliency maps. It will affect the image fusion quality. Fig. 2 (a)-(e) show the 5 steps of constructing saliency map in the proposed algorithm. As a second-order differential operator, Fig. 2 (a) shows that Laplacian filter has obvious advantages in enhancing image details. However, it will produce more noise than Sobel filter. We can see that the noise in the flat area is very significant. Fig. 2 (b) displays the sharpened image. The Sobel filter, as shown in Fig. 2(c), has stronger response in the area where the gray value changes drastically than the Laplacian filter. However, it has weaker response on noise and small details than the Laplacian filter. Hence, this noise can be smoothed by an average filter. The smoothed result is shown in Fig. 2 (d). The saliency map as shown in Fig. 2 (e) still retain details in the area where the gray value changes drastically. The noise is reduced in the area where the gray value changes are relatively flat.

The comparison results between the proposed method and GFF are shown in Fig. 3 and Fig. 4. Fig. 3 shows the comparison of the saliency maps generated by the proposed method and GFF. It can be clearly seen that the proposed method makes the edges in the saliency map sharper. Fig. 4(a) and (b) respectively display the fused images produced by our method and GFF. We enlarge the red frame area in the fused images and display them in Fig. 4(c) and Fig. 4(d). We can see that the fused image produced by GFF has more distortion compared to the fused image produced by our method. Therefore, by improving the method of constructing saliency maps, the quality of fused images is indeed improved.

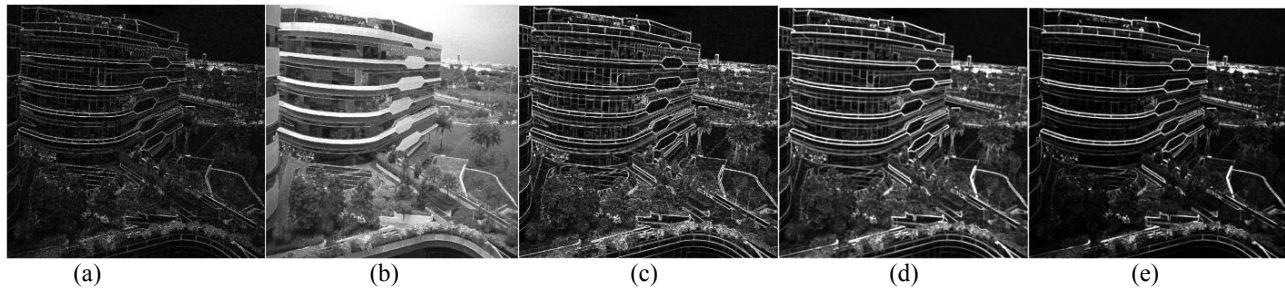


Fig. 2. (a) Applying Laplacian filtering to the source images; (b) Adding the source image to the image in (a); (c) Applying Sobel filter to the source image; (d) Applying mean filter to image in (c); (e) Multiplying images in (b) and (d)

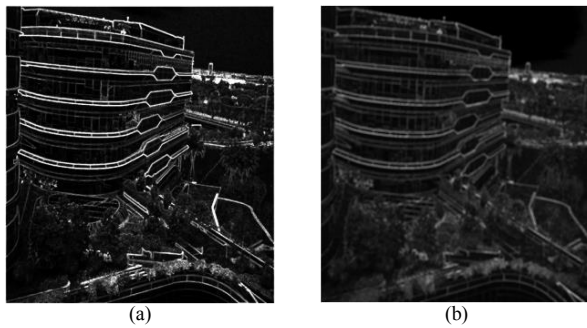


Fig. 3. Saliency map comparison using (a) the proposed method; (b) GFF;

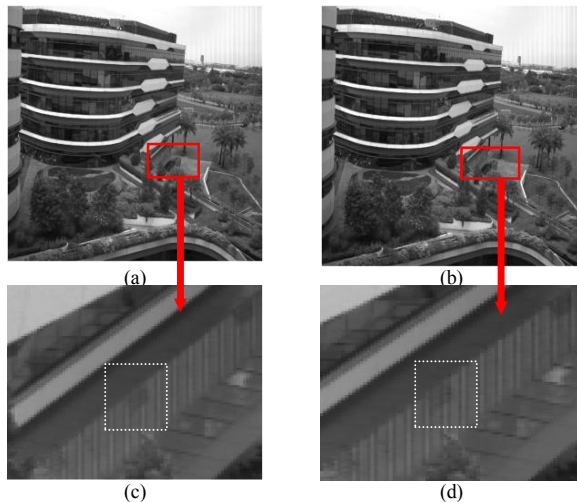


Fig. 4. Fusion results comparison using (a) the proposed; (b) GFF; (c) The enlarged red flame area in (a); (d) The enlarged red flame area in (b).

C. Computational Complexity and Processing Time

All the experiments are conducted with i5-10210U CPU at 2.8GHz, using MATLAB R2019b as the platform. Table II summarizes the complexity and processing time of GFF and the proposed method, for 1024×1024 images. The processing time in seconds are almost the same. By exploiting integral image technique [22], GFF has a linear time complexity as $O(N)$, where N is the total number of pixels in each source image. The complexity of the proposed method is also $O(N)$, because all the steps including the saliency map construction have complexity of $O(N)$. This shows that the proposed algorithm can significantly improve the fused image quality without computational complexity overhead.

TABLE II. THE COMPLEXITY AND THE PROCESSING TIME

Method	Computational Complexity	Processing Time (s)
GFF [12]	$O(N)$	3.87
Proposed	$O(N)$	4.00

V. CONCLUSION

In this paper, we propose an improved polarization image fusion method. This method uses self-guided image filtering to quickly complete multiscale decomposition, which is simple and effective. More importantly, by changing the ways of constructing saliency maps and the parameters of guided filtering, the method achieves spatial consistency and weight optimization. Objective comparison shows that the proposed algorithm can improve benchmarks Q_{MI} , Q_Y , Q_C and Q_P by around 4%, 3%, 12%, and 7% respectively. Together with subjective evaluation, the experimental results show that the proposed method can produce better fusion quality with little computation time overhead.

ACKNOWLEDGEMENT

This research was supported by Jiangsu Natural Science Foundation under grant 1004-PAC19009. This research was also supported by the Open Foundation of Graduate Innovation Base (Laboratory) of Nanjing University of Aeronautics and Astronautics under grant kfjj20200410.

REFERENCES

- [1] W. Bao, W. Wang and Y. Zhu, "Pleiades Satellite Remote Sensing Image Fusion Algorithm Based on Shearlet Transform," *Journal of The Indian Society of Remote Sensing*, vol. 46, no. 1, pp. 19-29, Jan. 2018.
- [2] B. Kunnen, C. Macdonald, A. Doronin, S. Jacques, M. Eccles and I. Meglinski, "Application of circularly polarized light for non-invasive diagnosis of cancerous tissues and turbid tissue-like scattering media," *Journal of Biophotonics*, vol. 8, no. 4, pp. 317-323, Apr. 2015.
- [3] H. Yi, L. Hu and Z. Fan, "A Polarization Image Fusion Method Based on Feature Analysis," *Journal of Applied Optics*, vol. 36, no. 02, pp. 220-226, Mar. 2015.
- [4] L. Zhang, F. Yang and L. Ji, "Infrared polarization and intensity image fusion algorithm based on the feature transfer," *Automatic Control and Computer Sciences*, vol. 52, no. 2, pp. 135-145, May 2018.
- [5] S. Li, D. Huang, H. Wang and T. Zou, "Polarization image fusion based on BEMD and adaptive PCNN," *Laser Journal*, vol. 39, no. 3, pp. 94-98, 2018.
- [6] X. Ji and G. Zhang, "Image fusion method of SAR and infrared image based on Curvelet transform with adaptive weighting," *Multimedia Tools Applications*, vol. 76, no. 17, pp. 17633-17649, Sep. 2017.

- [7] Y. Han, "Multimodal gray image fusion metric based on complex wavelet structural similarity," *Optik*, vol. 126, no. 8, pp. 5842-5844, Aug. 2015.
- [8] J. Zhang, Y. Zhang and Z. Shi, "Long-wave infrared polarization feature extraction and image fusion based on the orthogonality difference method," *Journal of Electronic Imaging*, vol. 27, no. 2, id. 023021, Apr. 2018.
- [9] R. Shen, I. Cheng, J. Shi, and A. Basu, "Generalized random walks for fusion of multi-exposure images," *IEEE Transactions on Image Processing*, vol. 20, no. 12, pp. 3634-3646, Dec. 2011.
- [10] M. Xu, H. Chen, and P. Varshney, "An image fusion approach based on markov random fields," *IEEE Transactions on Geoscience Remote Sensing*, vol. 49, no. 12, pp. 5116-5127, Dec. 2011.
- [11] K. L. Hua, H. C. Wang, A. H. Rusdi, and S. Y. Jiang, "A novel multifocus image fusion algorithm based on random walks," *Journal of Visual Communication and Image Represent*, vol. 25, no. 5, pp. 951-962, Jul. 2014.
- [12] S. Li, D. Xu and J. Hu, "Image Fusion with Guided filtering", *IEEE Transactions on Image Processing*, vol. 22, no. 7, Jul. 2013.
- [13] K. He, J. Sun, and X. Tang, "Guided image filtering," *IEEE Transactions on Pattern Analysis and Machine Intelligence*, vol. 35, no. 6, pp. 1397-1409, Jun. 2013.
- [14] W. Cao, H. W, J. Shi, R. Yu, and L. Tao, "Enhancement Algorithm of Finger Vein Image Based on Weighted Guided Filter with Edge Detection," *Laser and Optoelectronics Progress*, vol. 54, no. 02, pp. 172-180, Dec. 2017.
- [15] Z. Liu, "Research on target detection technology based on visible light polarization imaging," *Doctoral dissertation*, pp. 27-28, May 2016.
- [16] Gonzalez. Q. Ran, and Y. Ruan, *Digital Image Processing*, 2nd Edition, Beijing Electronic Industry Press, Aug. 2007.
- [17] I. Sobel and G. Feldman. "A 3x3 isotropic gradient operator for image processing," *a talk at the Stanford Artificial Intelligence Project*, 1968.
- [18] M. Hossny, S. Nahavandi, and D. Creighton, "Comments on 'information measure for performance of image fusion'," *Electronics Letters*, vol. 44, no. 18, pp. 1066-1067, Aug. 2008.
- [19] C. Yang, J. Zhang, X. Wang, and X. Liu, "A novel similarity based quality metric for image fusion," *Information Fusion*, vol. 9, no. 2, pp. 156-160, Apr. 2008.
- [20] N. Cvejic, A. Loza, D. Bull, and N. Canagarajah, "A similarity metric for assessment of image fusion algorithms," *International Journal of Signal Processing*, vol. 2, no. 3, pp. 178-182, Apr. 2005.
- [21] J. Zhao, R. Laganiere, and Z. Liu, "Performance assessment of combinative pixel-level image fusion based on an absolute feature measurement," *International Journal of Innovative Computing Information Control*, vol. 3, no. 6, pp. 1433-1447, Dec. 2007.
- [22] F. C. Crow, "Summed-area tables for texture mapping," in *Proceedings of the 11th Annual Conference Computer Graphics and Interactive Techniques*, pp. 207-212, Jan. 1984.